Energy Conversion and Management 258 (2022) 115526

Contents lists available at ScienceDirect

Energy Conversion and Management

journal homepage: www.elsevier.com/locate/enconman

Experimental comparison between various fitting approaches based on RMSE minimization for photovoltaic module parametric identification

Kari Lappalainen [a,*], Michel Piliougine [b], Giovanni Spagnuolo [b]

[a] Tampere University, Electrical Engineering Unit, 33720 Tampere, Finland
[b] University of Salerno, DIEM Department, 84084 Salerno, Italy

ARTICLE INFO

Keywords:
Parametric identification
Condition monitoring
Photovoltaic module
Single-diode model
Curve fitting
Series resistance

ABSTRACT

One solution for online condition monitoring of photovoltaic (PV) modules is to identify single-diode model parameter values from measured current–voltage (*I–V*) curves. By this way, use of expensive thermal cameras and radiometric sensors utilized in traditional monitoring methods can be avoided. Unfortunately, most of the parameter identification methods require measurements of the operating conditions, i.e., irradiance and temperature. This article proposes a novel procedure for identification of the single-diode model parameter values along with the operating irradiance and temperature values from measured *I–V* curves without needing any other measurement. The only inputs of the proposed procedure are the *I–V* curve measurements at the actual operating conditions together with the parameter values of the module model in standard test conditions. The proposed procedure is experimentally validated using *I–V* curves of three PV module types measured from two different locations. Both the whole *I–V* curves or only a part of them, in a limited voltage range, are considered. Moreover, *I–V* curve measurements with an emulated increase of the series resistance are used to demonstrate the correctness of the identified series resistance values. It is shown that the procedure identifies the operating irradiance and temperature with high accuracy even during sharp irradiance transitions and low irradiance conditions and identifies series and shunt resistances very reliably under nearly constant high irradiance conditions. Moreover, for the first time, a comprehensive comparison of various fitting approaches based on root-mean-square error (RMSE) minimization, including two novel approaches, is presented. The results show that the different fitting approaches based on RMSE minimization affect the accuracy of the parameters identification in a different way, this meaning that the used fitting approach is a factor that should be considered when implementing model parameter identification by curve fitting.

1. Intoduction

Online monitoring of photovoltaic (PV) modules condition, faults, aging and soiling is vital for operating PV power plants with the highest possible overall efficiency. Typically monitoring of PV modules relies on expensive methods using thermal cameras [1] or radiometric sensors [2] either in fixed installations or carried by drones. Thus, more efficient methods and tools are needed to reduce the maintenance and operation costs of PV power plants. One possible solution for online monitoring is to utilize measured current–voltage (*I–V*) curves, which can be modelled quite accurately under varying irradiance and temperature conditions using well-known electrical models, such as the single-diode model (SDM) and two-diode model. These models contain also condition and aging dependent parameters rendering condition monitoring based on parameters identification. The SDM is the most used electrical model providing a good trade-off between complexity and accuracy.

The values of the parameters appearing in the electrical models are usually identified in standard test conditions (STC), at which irradiance G and temperature T values are given, and then converted to other conditions based on their G and T behavior [3]. Several methods have been proposed for global and diffuse irradiance estimation. Comparisons of those methods are presented in [4,5]. However, the methods do not provide accurate enough estimates to be used in PV module parametric identification. Thus, appropriate environmental condition measurements are needed to identify parameter values under field conditions. Indeed, most of the presented parameter identification procedures require measurements of the operating conditions. For instance, measured ambient temperature or module backside temperature is used in [6], both irradiance and temperature are needed for the approaches

* Corresponding author.
E-mail addresses: kari.lappalainen@tuni.fi (K. Lappalainen), mpiliouginerocha@unisa.it (M. Piliougine), gspagnuolo@unisa.it (G. Spagnuolo).

https://doi.org/10.1016/j.enconman.2022.115526
Received 28 December 2021; Received in revised form 4 March 2022; Accepted 19 March 2022
Available online 1 April 2022

Nomenclature

α_{E_g}	thermal coefficient of energy band gap (1/K)
α_I	thermal coefficient of short-circuit current (A/K)
α_V	thermal coefficient of open-circuit voltage (V/K)
η	ideality factor (-)
η_{STC}	ideality factor at STC (-)
C_{STC}	coefficient calculated at STC (A/K^3)
$E_{g,\ STC}$	material energy band gap at STC (J)
G	irradiance (W/m^2)
G_{STC}	STC irradiance (W/m^2)
I	current (A)
$I_{MPP,\ STC}$	maximum power point current at STC (A)
I_{ph}	light-generated current (A)
$I_{ph,\ STC}$	light-generated current at STC (A)
I_s	dark saturation current (A)
$I_{s,\ STC}$	dark saturation current at STC (A)
I_{SC}	short-circuit current (A)
$I_{SC,\ STC}$	short-circuit current at STC (A)
k	Boltzmann constant (J/K)
N_s	number of series-connected PV cells in a PV module (-)
q	elementary charge (C)
R_s	series resistance (Ω)
$R_{s,\ STC}$	series resistance at STC (Ω)
R_{sh}	shunt resistance (Ω)
$R_{sh,\ STC}$	shunt resistance at STC (Ω)
T	temperature (K)
T_{STC}	STC temperature (K)
V	voltage (V)
$V_{MPP,\ STC}$	maximum power point voltage at STC (V)
V_{OC}	open-circuit voltage (V)
$V_{OC,\ STC}$	open-circuit voltage at STC (V)
V_t	thermal voltage (V)
$V_{t,\ STC}$	thermal voltage at STC (V)
W	Lambert W function

Abbreviations

MPP	maximum power point
OC	open-circuit
PL	power limit
PV	photovoltaic
RMSE	root-mean-square error
SC	short-circuit
SDM	single-diode model
STC	standard test conditions

presented in [7–11] and temperature is needed for the per-unit SDM-based method proposed in [12]. The need of operating condition measurements restricts the use of these methods for on-site condition monitoring. Only few procedures have been proposed earlier for parametric identification from measured *I–V* curves without the need for any other measurements. One such a procedure for SDM parameter identification was proposed in [13], which identifies the values of G and T along with the SDM parameter values. Instead of identifying multiple parameters, some methods focus on identification of the series resistance that is the most significant parameter for the assessment of the PV module state of health. An overview of these methods is given in [14]. In [15], a diagnostic method based on calculation of diagnostic indicators from *I–V* curves was proposed for detecting partial shading, increased series resistance and potential induced degradation of PV modules.

The SDM allows to simulate *I–V* curves via an implicit equation, which is often expressed in explicit form exploiting the Lambert W function [16]. Although the use of the explicit expression leads to lower accuracy compared to the use of the implicit equation, it is often preferrable due to lower computational burden. In addition to an accurate model, correct parameter values are vital for accurate modelling. During the last years, several deterministic [17] and stochastic [18,19] procedures have been proposed to calculate the SDM parameter values under given G and T conditions. A review of the parameter extraction methods was presented in [20] and 12 optimization algorithms for parameter estimation were compared in [21]. Some of the methods, like [22], utilize the whole *I–V* curve while some of them, like [23], require only the three most meaningful points of the curve, namely short-circuit (SC), open-circuit (OC) and maximum power point (MPP), in addition to the measured T and/or G. The deterministic methods can further be divided into numerical and analytical ones. In numerical methods, the exact solution of the SDM is calculated iteratively. A widely used numerical procedure is the one provided by Villalva et al. [24]. The analytical methods provide a complementary strategy where, under certain simplifications, the parameters are calculated by means of explicit equations [25]. A review of the analytical methods was presented in [26]. Moreover, an experimental validation of several explicit methods used for the SDM parameter identification was presented in [27], where the analysis focused on identification of series resistance in presence of artificial degradation.

Although several methods for SDM parameter extraction have been presented, only little attention has been paid to utilized fitting approaches based on root-mean-square error (RMSE) minimization. In general, all previous methods utilizing *I–V* curves aim to find a parameter set by which RMSE in I between the original and modelled *I–V* curve is minimized, by assuming that the simulated current is calculated at each voltage value where the real current was experimentally measured. This results from the fact that typically the current of the PV module is expressed as a function of the voltage, i.e., $I = f(V)$. However, the voltage of the PV module can be expressed as a function of the current, i.e., $V = f(I)$, as well. By that way, the curve fitting can be made based on minimization of RMSE in V instead of I, comparing the voltage coordinates of experimental and simulated points with the same current values. These two fitting approaches I and V have been compared earlier only in [28]. It was found therein that the recommended fitting approach is dependent on the method used to compute the *I–V* curve from the SDM. However, different fitting approaches based on RMSE minimization are not limited to these two, but other approaches can be formed by applying the I approach for one part of the curve and the V approach for other, e.g., the former at voltages that are lower than the MPP one and the latter between the MPP and the OC condition. In [28], the I and V approaches were compared using only 6 cases of single *I–V* curves. Thus, there is a need for a comprehensive study of fitting approaches based on RMSE minimization.

In this article, a novel procedure is proposed for the SDM parameter identification from measured *I–V* curves without the need for any other measurement. The proposed procedure identifies the SDM parameter values along with the values of G and T. Thus, the proposed procedure can be applied in on-site applications. Moreover, the procedure is implemented by four fitting approaches based on RMSE minimization, which are compared in terms of accuracy and computational costs. Validation of the proposed procedure and comparison of the fitting approaches is done using comprehensive sets of *I–V* curves of three PV modules measured at two different locations. Both the whole *I–V* curves or portions of them are considered. Moreover, *I–V* curve measurements after having added an external series resistance are used to estimate the correctness of the identified series resistance values. In this study, actual on-site *I–V* curve measurements are used while most of the earlier parameter identification procedures, like [11], have been validated

using I–V curves from manufacturers data sheets.

The main novelty of this study is twofold: (1) a novel procedure for SDM parameter identification from measured I–V curves without the need for G or T values is proposed and experimentally validated; and (2), for the first time, a comprehensive experimental comparison of various fitting approaches based on RMSE minimization, including two novel approaches, is presented. The proposed identification procedure is suitable for on-site applications facilitating online condition monitoring of PV modules. The results of this study show that the used fitting approach affects the obtained parameter values significantly, meaning that the used fitting approach is a factor that should be considered when implementing SDM parameter identification by curve fitting. Thus, the first comprehensive comparison of these approaches presented in this article is a worthwhile contribution to the current knowledge providing valuable information for development of parameter identification procedures. The results of this study are particularly relevant for parametric identification, condition monitoring and mathematical modelling of PV modules and systems.

The rest of this article is organized as follows. The proposed identification algorithm is introduced in Section 2.1, the studied fitting approaches are presented in Section 2.2 and the used measurement data is described in Section 2.3. Section 3.1 presents the results obtained by exploiting the entire I–V curves. The results obtained with portions of I–V curves, thus by using a subset of the experimental points they include, are presented in Section 3.2 and identification of the series resistance is further examined in Section 3.3 using I–V curves measured with additional series resistance values. The results and their significance are further discussed in Section 4. Finally, the conclusions of this study are provided in Section 5.

2. Methods and data

2.1. Identification algorithm

In this study, the basic implicit equations derived from the SDM are used to model PV modules. The most typical way is to express the current as a function of the voltage and current as.

$$I = I_{\mathrm{ph}} - I_{\mathrm{s}}\left(e^{\frac{V+R_{\mathrm{s}}I}{\eta V_{\mathrm{t}}}} - 1\right) - \frac{V + R_{\mathrm{s}}I}{R_{\mathrm{sh}}}, \tag{1}$$

where I_{ph} is the light-generated current, I_{s} the dark saturation current, R_{s} the series resistance, η the ideality factor and R_{sh} the shunt resistance of the PV module [25]. The thermal voltage V_{t} can be expressed as

$$V_{\mathrm{t}} = \frac{N_{\mathrm{s}}kT}{q}, \tag{2}$$

where N_{s} is the number of series-connected PV cells in the module, the Boltzmann constant is represented by k and q is the elementary charge. From Eq. (1) the following expression can be derived for the voltage as a function of the current and voltage

$$V = R_{\mathrm{sh}}I_{\mathrm{ph}} - R_{\mathrm{sh}}I_{\mathrm{s}}\left(e^{\frac{V+R_{\mathrm{s}}I}{\eta V_{\mathrm{t}}}} - 1\right) - (R_{\mathrm{s}} + R_{\mathrm{sh}})I. \tag{3}$$

The implicit equations (1) and (3) are used instead of the computationally less demanding explicit ones exploiting the Lambert W function since the purpose of this study is to compare fitting approaches based on RMSE minimization and thus the computational burden is not essential, but an iterative fitting method exploiting the implicit equations was considered to be more suitable for this purpose due to its higher accuracy. The equivalent circuit of a PV cell based on the SDM is presented in Fig. 1.

The set of identified parameters is $\{G, T, R_{\mathrm{s}}, R_{\mathrm{sh}}\}$. In order to identify these parameters from measured I–V curves using Eqs. (1) and (3), values for I_{ph}, I_{s} and η are required. The following procedure for obtaining these values is novel. The light-generated current I_{ph} can be

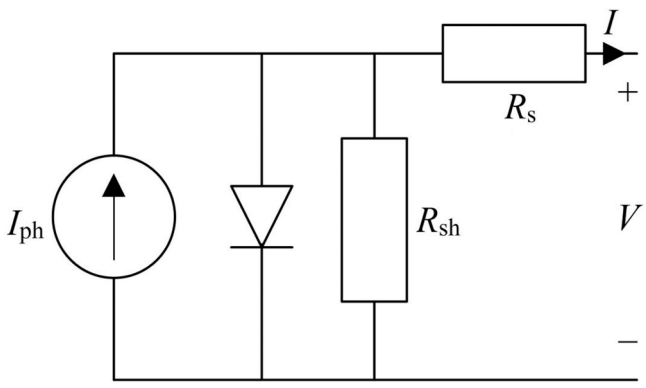

Fig. 1. SDM equivalent circuit of a PV cell.

calculated as

$$I_{\mathrm{ph}} = \frac{G}{G_{\mathrm{STC}}}\left(I_{\mathrm{ph,\,STC}} + \alpha_I(T - T_{\mathrm{STC}})\right), \tag{4}$$

where α_I is the thermal coefficient of I_{SC} [29]. This equation is usually applied with the assumption that $I_{\mathrm{ph,\,STC}} = I_{\mathrm{SC,\,STC}}$ [29]. However, instead of applying that simple assumption in the procedure here below, the effect of the parasitic resistances is taken into account by solving $I_{\mathrm{ph,\,STC}}$ as a function of $I_{\mathrm{SC,\,STC}}$ from Eq. (1) as

$$I_{\mathrm{ph,\,STC}} = I_{\mathrm{SC,\,STC}}\left(\frac{R_{\mathrm{sh}} + R_{\mathrm{s}}}{R_{\mathrm{sh}}}\right), \tag{5}$$

based on the widely used assumption [25,29] that in the SC condition I_{s} is negligible. Eq. (5) is then substituted to Eq. (4) leading to

$$I_{\mathrm{ph}} = \frac{G}{G_{\mathrm{STC}}}\left(I_{\mathrm{SC,\,STC}}\left(\frac{R_{\mathrm{sh}} + R_{\mathrm{s}}}{R_{\mathrm{sh}}}\right) + \alpha_I(T - T_{\mathrm{STC}})\right). \tag{6}$$

The ideality factor η was selected to remain fixed at its STC value [30], which is calculated as

$$\eta_{\mathrm{STC}} = \frac{\alpha_V - \frac{V_{\mathrm{OC,\,STC}}}{T_{\mathrm{STC}}}}{V_{\mathrm{t,\,STC}}\left(\frac{\alpha_I}{I_{\mathrm{ph,\,STC}}} - \frac{3}{T_{\mathrm{STC}}} - \frac{E_{\mathrm{g,\,STC}}}{kT_{\mathrm{STC}}^2}\right)}, \tag{7}$$

where α_V is the thermal coefficient of V_{OC} and $E_{\mathrm{g,\,STC}}$ is the material energy band gap at STC [31]. The saturation current I_{s} is calculated as

$$I_{\mathrm{s}} = C_{\mathrm{STC}}T^{3/\eta_{\mathrm{STC}}}e^{\frac{-E_{\mathrm{g}}(T)}{\eta_{\mathrm{STC}}kT}}, \tag{8}$$

where C_{STC} is a coefficient calculated at STC [32]. In the more common version of Eq. (8), η is assumed to be equal to 1 [29], but in the proposed procedure its value is computed as above. In OC and STC conditions, Eq. (1) can be written as

$$0 = I_{\mathrm{ph,\,STC}} - I_{\mathrm{s,\,STC}}\left(e^{\frac{V_{\mathrm{OC,\,STC}}}{\eta_{\mathrm{STC}}V_{\mathrm{t,\,STC}}}} - 1\right) - \frac{V_{\mathrm{OC,\,STC}}}{R_{\mathrm{sh}}}. \tag{9}$$

By neglecting the last term ($R_{\mathrm{sh}} \gg V_{\mathrm{OC,\,STC}}$) and the unitary term with respect to the exponential one in Eq. (9), I_{s} can be expressed as

$$I_{\mathrm{s,\,STC}} = I_{\mathrm{ph,\,STC}}e^{-\frac{V_{\mathrm{OC,\,STC}}}{\eta_{\mathrm{STC}}V_{\mathrm{t,\,STC}}}}. \tag{10}$$

By substituting Eq. (10) into Eq. (8), the coefficient C_{STC} can be solved as

$$C_{\mathrm{STC}} = \frac{I_{\mathrm{ph,\,STC}}e^{\gamma_{\mathrm{STC}}}}{T_{\mathrm{STC}}^{3/\eta_{\mathrm{STC}}}}, \tag{11}$$

where

$$\gamma_{\mathrm{STC}} = -\frac{V_{\mathrm{OC,\,STC}}}{\eta_{\mathrm{STC}} V_{\mathrm{t,\,STC}}} + \frac{E_{\mathrm{g,\,STC}}}{\eta_{\mathrm{STC}} k T_{\mathrm{STC}}}. \tag{12}$$

The energy bang gap is calculated as

$$E_{\mathrm{g}}(T) = E_{\mathrm{g,\,STC}}\left(1 + \alpha_{E_{\mathrm{g}}}(T - T_{\mathrm{STC}})\right), \tag{13}$$

where $\alpha_{E_{\mathrm{g}}}$ is the thermal coefficient of E_{g} [30].

For the actual curve fitting, guess values for the identified parameters $\{G, T, R_{\mathrm{s}}, R_{\mathrm{sh}}\}$ are required. For all I–V curves, except the first of each dataset, the identified parameter set of the previous curve is used as guess values, given that the time interval between two consecutive curve acquisitions is not too long. For the first curve of each dataset, STC values of $\{G, T, R_{\mathrm{s}}, R_{\mathrm{sh}}\}$ are used as their initial guesses. The STC values of R_{s} and R_{sh} are calculated by the following procedure. First, the $I_{\mathrm{ph,\,STC}}$ is assumed to be $I_{\mathrm{SC,\,STC}}$. Secondly, η_{STC} is calculated by Eq. (7). After that, $I_{\mathrm{s,\,STC}}$ is obtained using Eq. (8) with the STC values of T, η and E_{g}. Finally, the STC values for the parasitic resistances are calculated by the procedure presented in [25]: the STC values for R_{s} and R_{sh} are obtained by

$$R_{\mathrm{s,\,STC}} = \frac{x\eta_{\mathrm{STC}} V_{\mathrm{t,\,STC}} - V_{\mathrm{MPP,\,STC}}}{I_{\mathrm{MPP,\,STC}}} \tag{14}$$

and

$$R_{\mathrm{sh,\,STC}} = \frac{x\eta_{\mathrm{STC}} V_{\mathrm{t,\,STC}}}{I_{\mathrm{ph,\,STC}} - I_{\mathrm{MPP,\,STC}} - I_{\mathrm{s,\,STC}}(e^{x} - 1)}, \tag{15}$$

where x is computed utilizing the Lambert W function as

$$x = W\left[\frac{V_{\mathrm{MPP,\,STC}}\left(2I_{\mathrm{MPP,\,STC}} - I_{\mathrm{ph,\,STC}}\right) e^{\frac{V_{\mathrm{MPP,\,STC}}\left(V_{\mathrm{MPP,\,STC}} - 2\eta_{\mathrm{STC}} V_{\mathrm{t,\,STC}}\right)}{\eta_{\mathrm{STC}}{}^{2} V_{\mathrm{t,\,STC}}{}^{2}}}}{\eta_{\mathrm{STC}} I_{\mathrm{s,\,STC}} V_{\mathrm{t,\,STC}}}\right] + 2\frac{V_{\mathrm{MPP,\,STC}}}{\eta_{\mathrm{STC}} V_{\mathrm{t,\,STC}}} - \frac{V_{\mathrm{MPP,\,STC}}{}^{2}}{\eta_{\mathrm{STC}}{}^{2} V_{\mathrm{t,\,STC}}{}^{2}}. \tag{16}$$

The proposed procedure is illustrated in Fig. 2.

2.2. Fitting approaches based on RMSE minimization

Traditionally PV module I–V curves are modelled by calculating I for the given values of V. Correspondingly the curve fitting of SDM is typically made based on minimization of RMSE in I, by assuming that the simulated I–V curve is computed at the same experimental voltage values at which the current was measured. The opposite solution is to calculate V for each given value of I and fit the curve based on minimization of the RMSE in V. In the following, these two fitting approaches are called approaches I and V, respectively. In addition to these two approaches, combinations of them can be formed by applying the I approach for one part of the I–V curve and the V approach for other. One justified way is to apply different approaches for different branches of the measured I–V curve, at the left side and at the right side of the MPP. That might be advantageous for identifying the parasitic resistances as the series resistance is related to the slope of the curve at voltages higher than the MPP voltage (right side of the MPP) whereas the shunt resistance depends on the slope of the curve at voltages lower than the MPP voltage (left side of the MPP).

Two novel fitting approaches combining the I and V strategies are proposed and compared with the I and V approaches. In the $I\&V$ approach, the RMSE in I is minimized on the left side of the measured MPP and the RMSE in V is minimized on the right side of the MPP. In the $V\&I$ approach, the opposite approach is applied: the RMSE in V is minimized on the left and the RMSE in I on the right side of the MPP. There are some factors that might impede the use of combined RMSE computation approaches and thus need to be taken into account: I and V values of I–V curves usually differ by one order of magnitude (V values are typically larger than I values) and the number of experimental $\{I, V\}$ pairs on the left and right side of the MPP is not the same. Due to these factors, RMSE values on one side of the MPP are larger than on the other side, and thus one side of the MPP will have larger weight on the total RMSE of the curve than the other side, i.e., there will be uneven weighting. In order to avoid this effect, the I and V values need to be normalized before curve fitting. In the $I\&V$ approach, the I values are divided by I_{MPP} and the share of points in the right side of the MPP, while the V values are divided by V_{MPP} and the share of points on the left side of the MPP. In the $V\&I$ approach, the I values are divided by I_{MPP} and the share of points in the left side of the MPP, and the V values are divided by V_{MPP} and the share of points on the right side of the MPP. The values of $I_{\mathrm{SC,\,STC}}$, $V_{\mathrm{OC,\,STC}}$, $I_{\mathrm{MPP,\,STC}}$ and $V_{\mathrm{MPP,\,STC}}$ used in the curve fitting are normalized correspondingly. Values of α_I and α_V are set in proportion to the normalized $I_{\mathrm{SC,\,STC}}$ and $V_{\mathrm{OC,\,STC}}$, and the rest of the parameter values are calculated by the procedure of Section 2.1 using the normalized values.

The examined fitting approaches are compared in terms of identified parameter values, computation costs (numbers of iterations and function evaluations) and the relative area between the measured and fitted curves with respect to the area of the measured curve. The identified G and T values are compared to the measured ones in Sections 3.1 and 3.2 and I–V curve measurements with additional R_{s} are used to estimate the correctness of the identified R_{s} values in Section 3.3. Comparison in terms of the obtained RMSE values does not make sense since the variable relative to which the RMSE is calculated determines which approach has the lowest RMSE, i.e., if the RMSE is calculated with respect to I, the I approach has the lowest RMSE and so on. Thus, the areas between the measured and fitted curves are calculated to compare accuracies of the curve fits obtained with different fitting approaches.

2.3. Measurement data

Validation of the proposed SDM parameter identification procedure and comparison of the fitting approaches based on RMSE minimization is done utilizing four sets of I–V curves measured from three different PV modules. Two datasets are from the University of Malaga, Spain and two datasets are from Tampere University, Finland. First, parameter identification using entire I–V curves is studied with two datasets. The first dataset consists of 55 I–V curves of a ISOFOTON I-53 module measured in Malaga on 29 July 2017. The second dataset consists of 900 I–V curves of a NAPS NP190GK module measured in Tampere on 21 August 2020. Parameter identification using only a part of the I–V curves is demonstrated using a set of 20 I–V curves of a ISOFOTON ISF-145 module measured in Malaga on 14 July 2014. Finally, identification of R_{s} is further examined using a set of 300 I–V curves of the NAPS NP190GK module in Tampere. This set consist of two subsets of 100 curves measured with additional R_{s} of 0.22 and 0.69 Ω on 16 and 31 July 2020, respectively, and 100 curves measured without additional R_{s} on 26 August 2020. The PV cells used in the I-53 and ISF-145 modules are fabricated of monocrystalline silicon while the NP190GK is composed of polycrystalline silicon PV cells. The use of measured I–V curves of

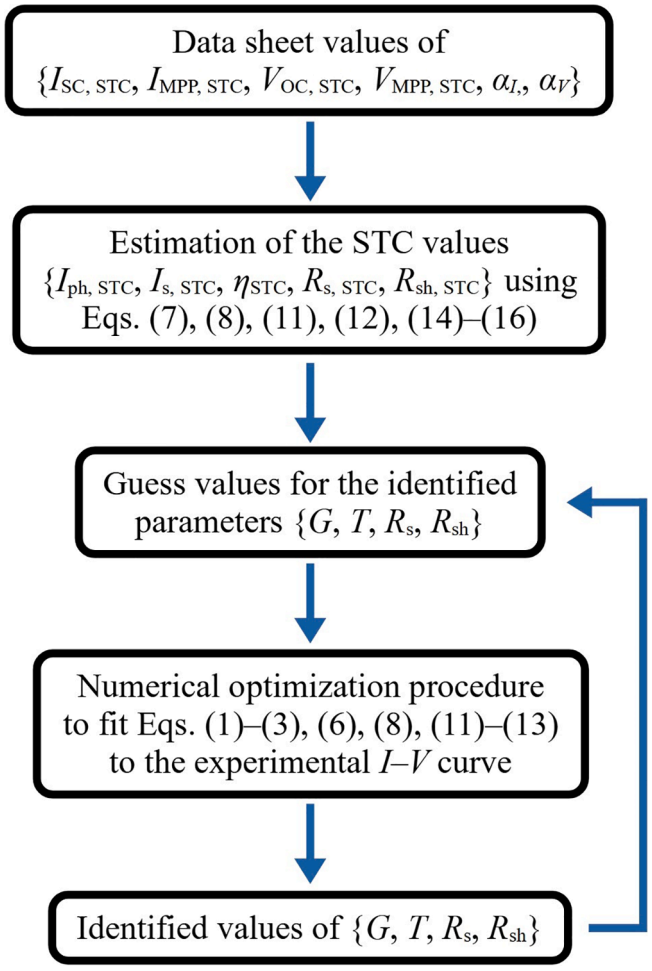

Fig. 2. Flowchart of the proposed identification procedure.

several PV modules demonstrates that the proposed SDM parameter identification procedure can be applied to different PV modules.

Time intervals between the measurements of the I-53 and ISF-145 modules were from 6 to 7 s and from 9 to 10 s, respectively. The I–V curves of the I-53 and ISF-145 modules consist of 88 and 74 {I, V} pairs on average, respectively. On-plane incident irradiance values were measured by CMP21 pyranometers (Kipp & Zonen) and PV module back-sheet temperatures were measured by Pt100 temperature sensors. A detailed description of the University of Malaga measurement system is presented in [33]. The I–V curves of the NAPS NP190GK module were measured once per second using an I–V curve tracer utilizing the electronic load method [34]. The I–V curve tracer is located inside a laboratory and thus the measurements are done through cables having a total resistance of 0.363 Ω. The I–V curves were pre-processed by the procedure provided in [35] after which the points with identical measured voltage value were replaced with a single point by averaging their measured current values. The pre-processed curves consist of 657

Table 1
Electrical parameter values of the studied PV modules.

Variable	ISOFOTON I-53	ISOFOTON ISF-145	NAPS NP190GK
$I_{SC,\,STC}$ (A)	2.56	8.55	8.72
$V_{OC,\,STC}$ (V)	20.5	22.4	32.8
$I_{MPP,\,STC}$ (A)	2.26	8.00	7.94
$V_{MPP,\,STC}$ (V)	16.5	18.1	22.9
α_I (A/K)	0.00102	0.00359	0.0047
α_V (V/K)	−0.061	−0.072	−0.124
N_s	36	36	54

Table 2
SDM parameters of the studied PV modules at STC.

Variable	ISOFOTON I-53	ISOFOTON ISF-145	NAPS NP190GK
$I_{ph,\,STC}$ (A)	2.56	8.55	8.72
η_{STC} (-)	0.88541	1.0041	1.0655
$I_{s,\,STC}$ (A)	3.4425e-11	2.8646e-10	2.0145e-9
$R_{s,\,STC}$ (Ω)	0.60181	0.18235	0.70927
$R_{sh,\,STC}$ (Ω)	90.167	131.43	96.994

Table 3
Initial guess solutions and ranges of the four identified parameters for the studied PV modules.

Parameter	ISOFOTON I-53	ISOFOTON ISF-145	NAPS NP190GK
G (W/m^2)	1000 [10, 1300]	1000 [10, 1300]	1000 [10, 1300]
T (°C)	25 [0, 70]	25 [0, 90]	25 [0, 70]
R_s (Ω)	0.60181 [0.1, 5]	0.18235 [0.05, 5]	0.70927 [0.1, 5]
R_{sh} (Ω)	90.167 [5, 500]	131.43 [5, 700]	96.994 [50, 800]

{I, V} pairs on average. An SP Lite2 pyranometer (Kipp & Zonen), mounted at the same 45° tilt angle as the module, was used to measure irradiance incident on the module. Back-sheet temperature of the module was measured by a Pt100 temperature sensor. A detailed description of the Tampere University measurement system is presented in [36].

The electrical parameter values used in this work for the studied PV modules are presented in Table 1. The datasheet values provided by the manufacturer were used for the ISF-145 module. It was noticed that the values provided by the manufacturers for the I-53 and NP190GK modules, which have been working for a long time, are not close to the real ones. Thus, the values determined in [37] and [38] were used for the I-53 and NP190GK modules, respectively. These values were determined based on measurements done near the measurements used in this study. Thus, those values are valid for the study presented in this article.

The SDM parameters at STC calculated for the studied PV modules are summarized in Table 2. The initial guess solutions and ranges of the identified parameters {G, T, R_s, R_{sh}} are presented in Table 3 for the studied PV modules. Due to the short time intervals between consecutive I–V curve measurements, the identified set of parameters {G, T, R_s, R_{sh}} of the previous curve is used as the guess solutions from the second curve onwards.

3. Experimental results

3.1. Parameter identification using entire I–V curves

In the first identification example, values for the parameter set {G, T, R_s, R_{sh}} were identified for 55 I–V curves of the ISOFOTON I-53 module.

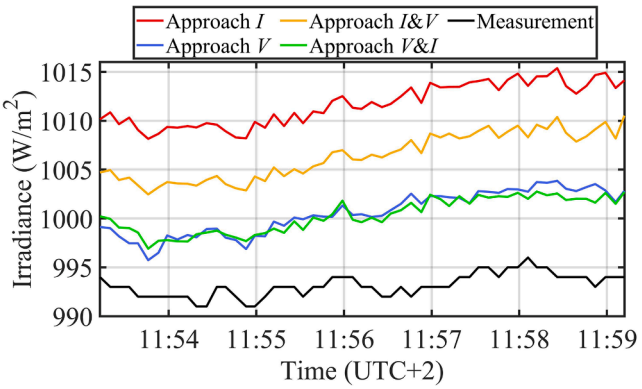

Fig. 3. Identified and measured irradiances for the set of 55 I-53 module I–V curves.

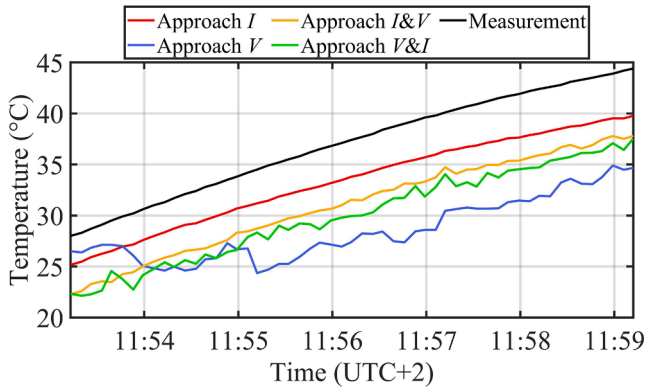

Fig. 4. Identified cell temperatures and measured module backside temperatures for the set of 55 I-53 module *I–V* curves.

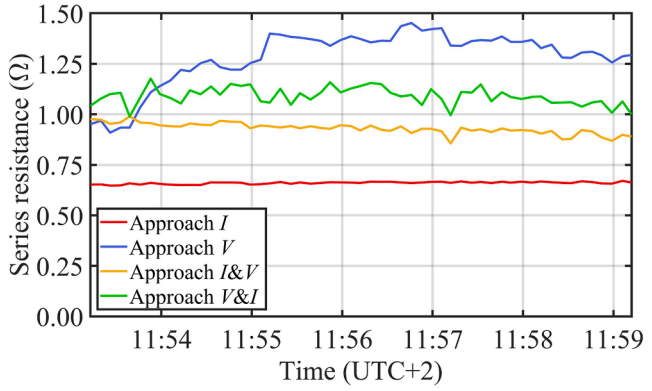

Fig. 5. Identified series resistances for the set of 55 I-53 module *I–V* curves.

The identified and measured irradiances are presented in Fig. 3. The measured irradiance is quite constant during the studied period, varying between 991 and 996 W/m^2. All the studied fitting approaches based on RMSE minimization reproduce the shape of the measured irradiance curve nicely with some overestimation. The overestimation is the smallest for the *V* and *V&I* approaches and the largest for the *I* approach. However, even the largest overestimations are only around 2% of the measured irradiance.

Fig. 4 presents the identified and measured temperatures for the I-53 module *I–V* curves. All the fitting approaches somewhat underestimate the measured temperature. The *I* approach provides the most accurate identified temperature with an average difference of 3.6 °C or 1.2% from the measured values. Moreover, the *I* approach provides the smoothest irradiance while the irradiances identified by the other approaches,

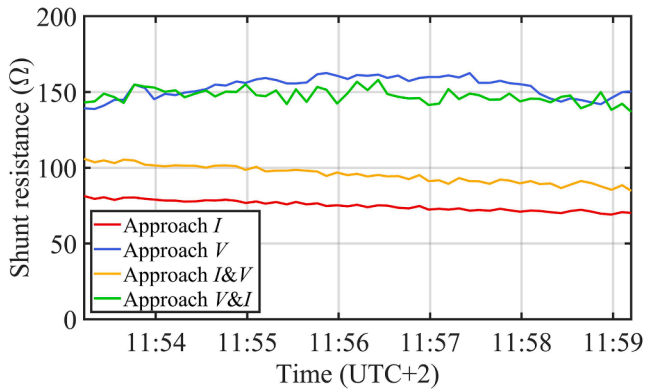

Fig. 6. Identified shunt resistances for the set of 55 I-53 module *I–V* curves.

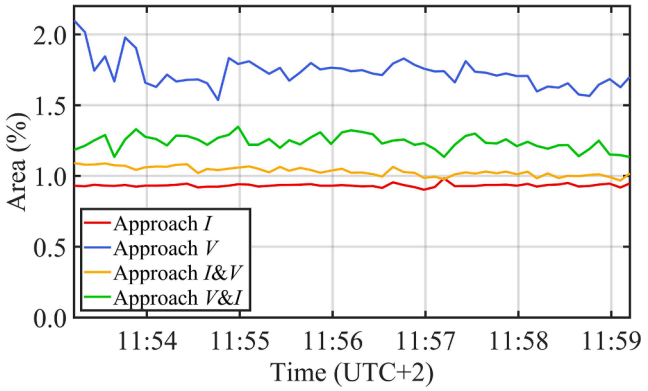

Fig. 7. Areas between the measured and fitted curves with respect to the area of the measured curve for the set of 55 I-53 module *I–V* curves.

Table 4
Computation costs of the studied fitting approaches for the set of 55 I-53 module *I–V* curves.

Approach	Average number of iterations	Average number of function evaluations
I	20.7	108
V	21.8	114
I&V	22.1	116
V&I	22.8	119

especially the *V* approach, show more fluctuations. The *V* approach is the only one failing to reproduce the shape of the measured temperature curve.

In addition to the operating irradiance and temperature also the values of the parasitic resistances were identified. The identified series and shunt resistance are presented in Figs. 5 and 6, respectively. The *I* approach provides the smallest resistance values with the smallest variation. The *I&V* approach gives the second smallest values with small variation, while the resistance values provided by the *V* and *V&I* approaches show somewhat larger variation. However, all the approaches identify stably the shunt resistance. The series resistance values identified by the *I* approach are close to the STC value of Table 2 similarly than the shunt resistance values identified by the *I* and *I&V* approaches.

As stated in Section 2.2, the accuracy of the fitting approaches is compared in terms of the relative area between the measured and fitted curves with respect to the area of the measured curve. The areas are presented in Fig. 7 for the I-53 module *I–V* curves. All the approaches show good accuracy in terms of the relative area between the measured and fitted curves. However, the smallest areas are achieved by the *I* and *I&V* approaches. Moreover, the areas achieved by these approaches are

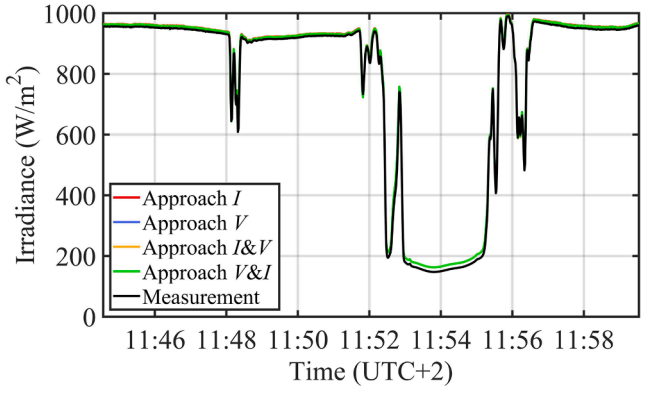

Fig. 8. Identified and measured irradiances for the set of 900 NP190GK module *I–V* curves.

very stable. The largest variation together with the largest values exists in the areas of the *V* approach.

The numbers of iterations and function evaluations for the studied approaches are listed in Table 4 for the I-53 module *I–V* curves. These values indicate that the *I* approach is computationally the least demanding while the *V&I* approach has the highest computational burden. However, the differences between the approaches are small.

In the second identification example, 900 *I–V* curves of the NAPS NP190GK were examined. The curves were measured once a second during a period of 15 min. The selected period involves a wide range of different operating conditions. The identified and measured irradiances are presented in Fig. 8. The measured irradiance is quite constant on a high level for the first three minutes after which some shading occurs decreasing the irradiance to around 600 W/m^2. The shadings are followed by other three minutes of high irradiance conditions after which a longer shading period exist followed by nearly constant high irradiance conditions at the end of the period. Despite of the sharp irradiance transitions, all the approaches success to follow the shape of the measured irradiance with slight overestimation.

Accuracy of the identified irradiance values is further illustrated in Fig. 9 where the differences between the identified and measured irradiances are presented. During the constant high irradiance conditions, all the identified irradiances are within 1.3% from the measured irradiance. In these conditions, the irradiance overestimation is the smallest for the *V* and *V&I* approaches and the largest for the *I* approach similarly than in the first identification example. During the constant low irradiance conditions around 11:54, all the identified irradiances are about 15 W/m^2 or 9% higher than the measured value and there are only minor differences between the approaches. As expected, the largest differences between the identified and measured irradiance values exist during sharp irradiance transitions. In order to further illustrate the behavior of the identified irradiances, the irradiance identified by the *I* approach is presented in Fig. 10 as a function of the measured irradiance. Fig. 10 confirms the slight irradiance overestimation and shows that the identified irradiance values are close to the measured ones along the whole irradiance range.

The identified and measured temperatures are presented in Fig. 11 for the NP190GK module *I–V* curves. The operating temperature of a PV module is naturally dependent on the irradiance incident on the module. The measured temperature decreases about 10 °C during the shading period around 11:54. However, the irradiance transitions around 11:48 were so fast that they did not cause a temperature drop. All the fitting approaches somewhat underestimate the measured temperature similarly than in the first identification example (see Fig. 4). Again, the *I* approach provides the most accurate identified temperature. However, the differences between the approaches are smaller than in the first identification example. All the approaches success to follow the shape of the measured irradiance, apart from the sharp irradiance transitions

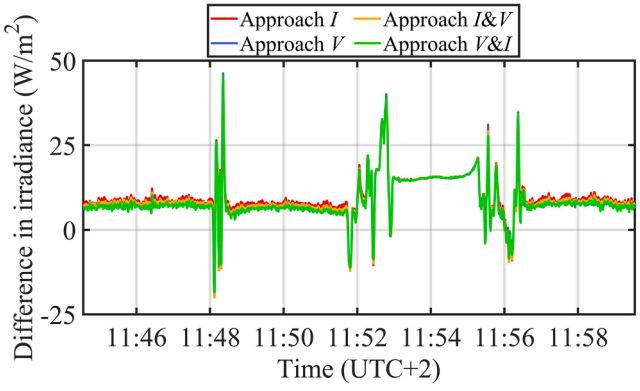

Fig. 9. Differences between the identified and measured irradiances for the set of 900 NP190GK module *I–V* curves.

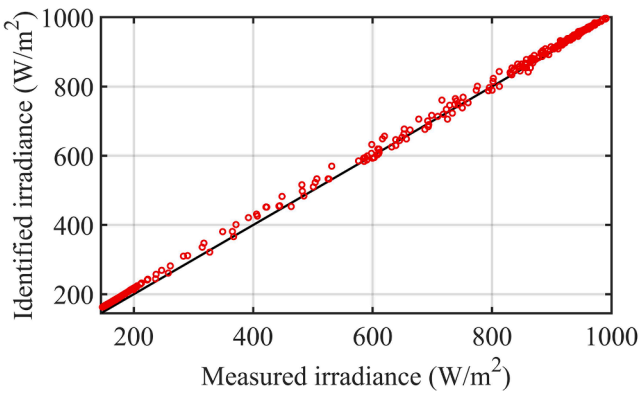

Fig. 10. Scatter plot between the irradiance identified by the *I* approach and the measured irradiance for the set of 900 NP190GK module *I–V* curves.

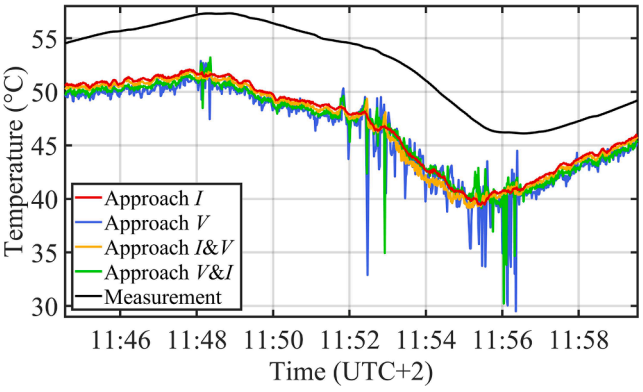

Fig. 11. Identified cell temperatures and measured module backside temperatures for the set of 900 NP190GK module *I–V* curves.

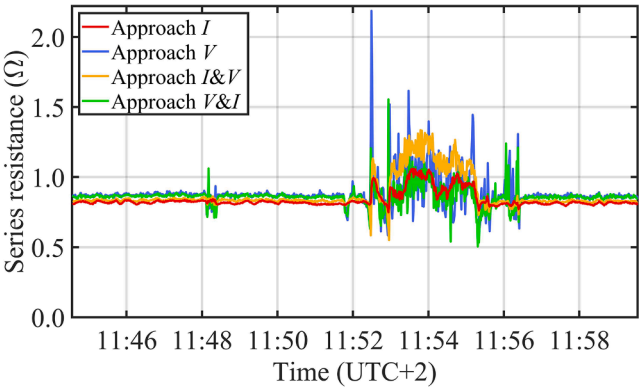

Fig. 12. Identified series resistances for the set of 900 NP190GK module *I–V* curves.

which cause large variation in the temperature identified by the *V* and *V&I* approaches. Only few small peaks exist in the temperature identified by the *I&V* approach while the *I* approach provides stable identified temperature even during the fastest irradiance transitions.

The series and shunt resistance identified for the NP190GK module *I–V* curves are presented in Figs. 12 and 13, respectively. Again, the *I* approach provides the most stable identified resistances with the smallest values. All the approaches identify resistance values higher than the STC values of Table 2, the values identified by the *I* approach being closest to the STC values. The differences in identified series resistance values between the approaches are smaller than in the first

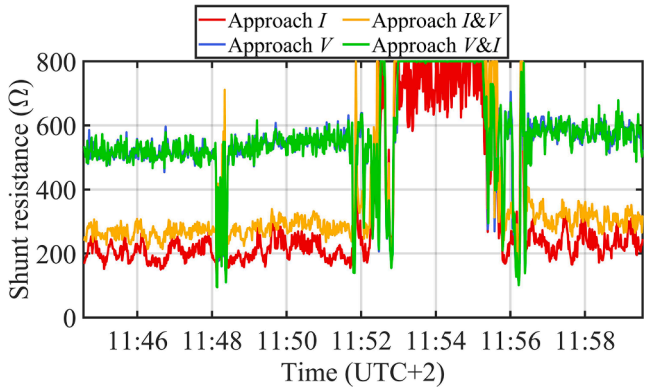

Fig. 13. Identified shunt resistances for the set of 900 NP190GK module *I–V* curves.

identification example. The series resistances identified by the *V*, *I&V* and *V&I* approaches vary largely during the sharp irradiance transitions. However, the *I* approach provides quite stable identified value even during the irradiance transitions. During the short medium irradiance conditions around 11:48 and 11:56, the identified shunt resistances of the *I* and *I&V* approaches have higher values than during the constant high irradiance conditions. That kind of behavior was achieved also by other procedures proposed in previous literature [13,39]. In both of these approaches, the current was expressed as a function of the voltage in explicit form, i.e., the *I* approach was used. However, by the *V* and *V&I* approaches lower shunt resistance values are obtained during the medium conditions than during the constant high irradiance conditions. This demonstrates that the used fitting approach has a great effect on the obtained shunt resistance values. In some cases, during the longer shading period around 11:54, the identified shunt resistance values reach the upper bound of Table 3 in line with the results shown in [13]. This happens most often with the *V&I* approach and is most rare for the *I* approach. However, during high irradiance conditions, the proposed identification procedure identifies stably the shunt resistance. Indeed, during the constant high irradiance conditions, the identified shunt resistances of all the approaches are much more stable than the ones obtained for the same NP190GK module in [13].

Fig. 14 shows the relative areas between the measured and fitted curves for the NP190GK module *I–V* curves. All the approaches show good accuracy under constant irradiance conditions, even during the shading period around 11:54. Indeed, the relative areas for the NP190GK module are smaller than for the I-53 module in the first identification example. Relative areas of over 1% occur for the *V* and *V&I* approaches during the irradiance transitions. The largest relative areas for the *I* and *I&V* approaches are 0.60% and 0.77%, respectively.

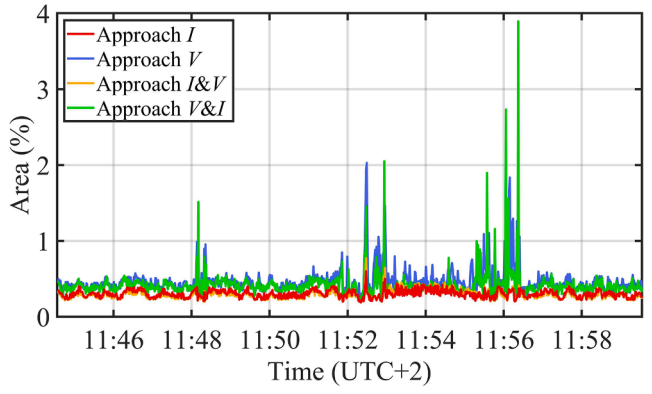

Fig. 14. Areas between the measured and fitted curves with respect to the area of the measured curve for the set of 900 NP190GK module *I–V* curves.

Table 5
Computation costs of the studied approaches for the set of 900 NP190GK module *I–V* curves.

Approach	Average number of iterations	Average number of function evaluations
I	24.7	128
V	27.4	142
I&V	23.2	121
V&I	28.1	146

Moreover, the relative areas for these approaches are much more stable than those for the *V* and *V&I* approaches.

The numbers of iterations and function evaluations for the studied approaches are compiled in Table 5 for the NP190GK module *I–V* curves. These values indicate that in this identification example the *I* and *I&V* approaches are computationally less demanding than the *V* and *V&I* approaches. The numbers of iterations and function evaluations in Table 5 are larger than those for the I-53 module *I–V* curves in Table 4, which is reasonable since the NP190GK module *I–V* curves consist of a larger number of measurement points than the I-53 module *I–V* curves.

3.2. Parameter identification using portions of the I–V curves

In this identification example, 20 *I–V* curves of the ISOFOTON ISF-145 module were examined to demonstrate parameter identification using only a part of the measured *I–V* curve. In practical applications, ideal condition monitoring would be based on *I–V* curve measurements performed in the vicinity of the MPP, so that a small power drop is required to perform the identification action. In order to define an adequate share of the *I–V* curves near the MPP for feasible parameter identification, the results are presented as a function of power limit (PL). The PL gives the power, with respect to the MPP power, from which the curve is cut so that only the points with power higher than the PL are utilized for the identification. The power limit was varied from 0% (all the samples of the *I–V* curve are used for the identification) to 99% (only the points within 1% from the MPP power). The operating conditions of the module are almost fixed over the measurement period: the irradiance varied only slightly between 903 and 905 W/m^2 and the temperature increased marginally being between 50.3 and 51.5 °C.

The average differences between the identified and measured irradiances are shown in Fig. 15 for the 20 curves. The results are promising showing that the operating irradiance can be identified reliably using only the points within 20% of the maximum power. Again, all the approaches identify irradiances higher than the measured values and the largest overestimation corresponds to the *I* approach. Fig. 16 presents the average differences between the identified cell temperatures and measured module backside temperatures for the 20 ISF-145 module *I–V*

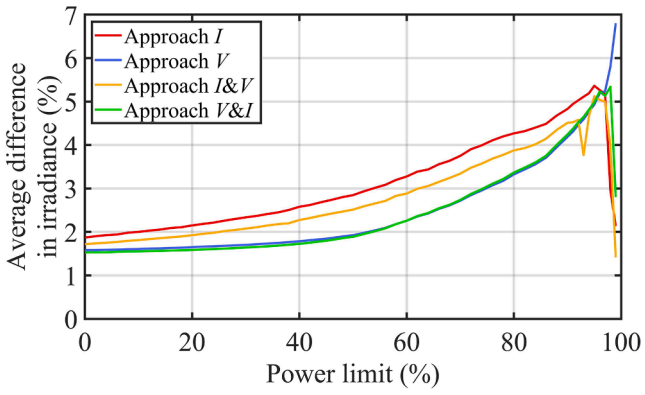

Fig. 15. Average differences in the identified irradiances with respect to the measured irradiance for the set of 20 ISF-145 module *I–V* curves as a function of the power limit.

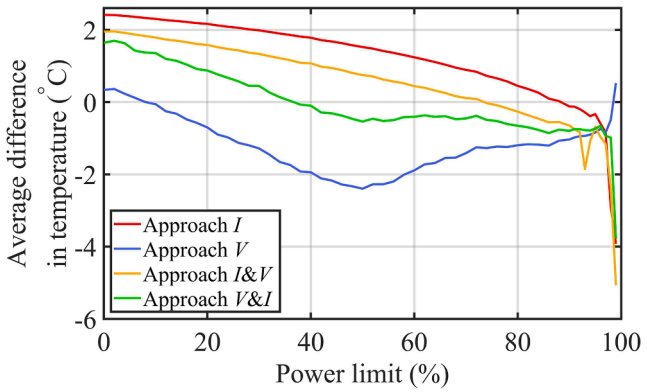

Fig. 16. Average differences between the identified cell temperatures and the measured module backside temperature for the set of 20 ISF-145 module *I–V* curves as a function of the power limit.

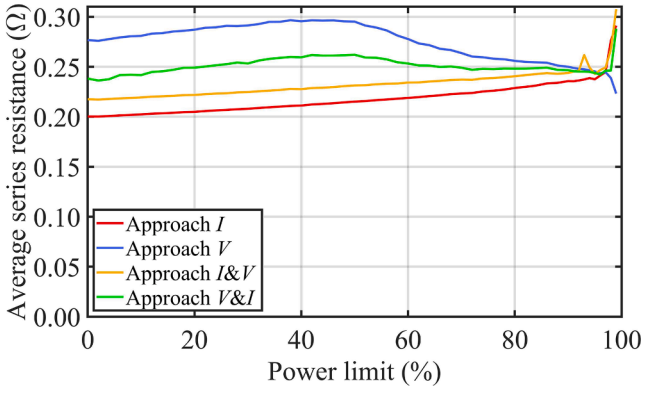

Fig. 17. Average identified series resistances for the set of 20 ISF-145 module *I–V* curves as a function of the power limit.

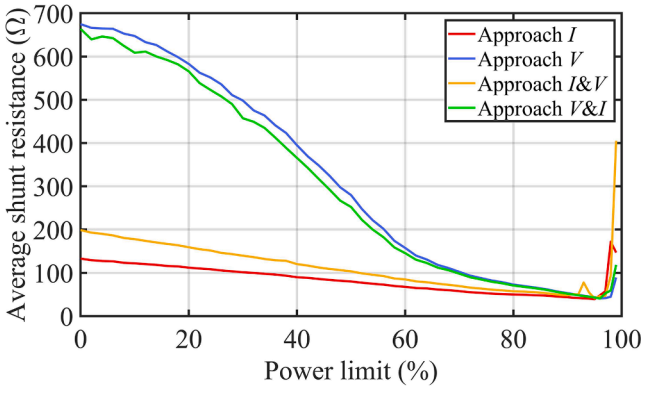

Fig. 18. Average identified shunt resistances for the set of 20 ISF-145 module *I–V* curves as a function of the power limit.

curves. Also these results are promising: the identified irradiances of all the approaches are within 2.5 °C from the measured one with a broad power limit range from 0% to 97%. Again, the *I* approach provides the highest and the *V* approach the lowest identified temperature levels.

The average identified series and shunt resistances are presented in Figs. 17 and 18, respectively, for the 20 ISF-145 module *I–V* curves. The identified series resistances in Fig. 17 are quite constant through the whole power limit range indicating that the series resistance can be identified accurately from measurements performed in the vicinity of the MPP. The shunt resistances identified by the *I* and *I&V* approaches

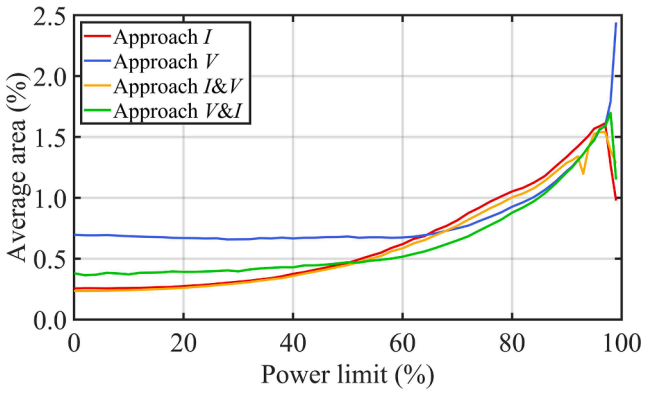

Fig. 19. Average areas between the measured and fitted curves with respect to the area of the measured curve for the set of 20 ISF-145 module *I–V* curves as a function of the power limit.

decrease almost linearly with the increasing power limit until they increase rapidly with very high power limits. The decrease of the identified shunt resistance while the power limit increases from 0% to 60% is faster for the *V* and *V&I* approaches than for the *I* and *I&V* approaches. With power limits from 70% to 95%, the identified shunt resistances of all the approaches are close to each other. Again, the smallest resistance values are identified by the *I* approach.

Fig. 19 shows the average relative areas between the measured and fitted curves as a function of the power limit for the 20 ISF-145 module *I–V* curves. When most of the curves (power limit below 50%) is used for the parameter identification, the *I* and *I&V* approaches have the smallest areas between the measured and fitted curves. At power limits from 52% to 92%, the *V* approach has the smallest area. However, the differences between the approaches are small at power limits higher than 50%. The areas of all the approaches increase with increasing power limit except that at very high power limits the areas of the *I*, *I&V* and *V&I* approaches decrease with increasing power limit. For all the approaches, the average relative area between the measured and fitted curves is less than 1.5% at power limits less than 94%. The small areas between the measured and fitted curves even with high power limits indicate that the proposed identification procedure provides accurate curve fits and can be used for condition monitoring utilizing *I–V* curve measurements performed only in the vicinity of the MPP. This is an important finding demonstrating suitability of the proposed procedure for practical applications.

3.3. Identification of a varying series resistance

In order to demonstrate the ability of the proposed procedure to

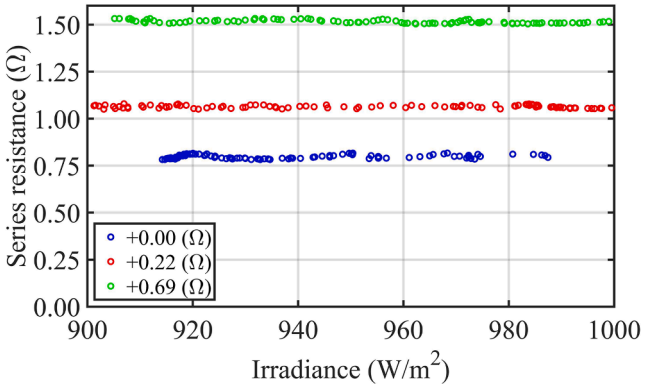

Fig. 20. Series resistances identified by the *I* approach for the set of NP190GK module *I–V* curves with additional resistances.

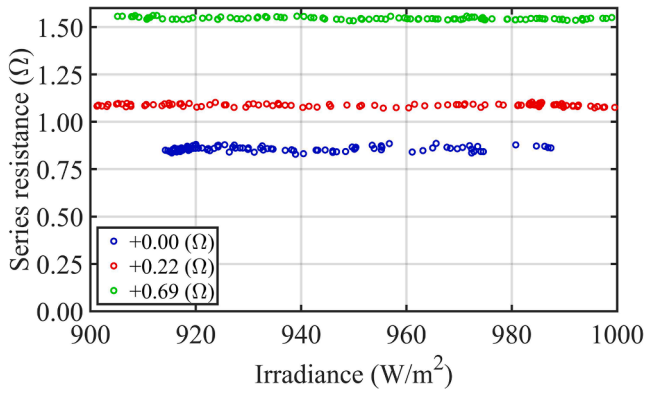

Fig. 21. Series resistances identified by the *V* approach for the set of NP190GK module *I*–*V* curves with additional resistances.

identify the actual value of the series resistance, NP190GK module *I*–*V* curves obtained by adding an additional resistance at the module terminals were examined. The examined *I*–*V* curve set consists of two subsets of 100 curves measured with additional resistance of 0.22 and 0.69 Ω. For sake of comparison, the third subset consists of 100 curves measured without additional resistance. In each case, the irradiance incident on the module increased slowly from around 900 W/m^2 to around 1000 W/m^2. Figs. 20 and 21 show the series resistance values identified by the *I* and *V* approaches, respectively, as a function of the measured irradiance. Both approaches identify stably the three resistance levels. The obtained resistance values are in accord with the results shown in [40]. In line with the three earlier identification examples, the *I* approach identifies somewhat lower series resistance values than the *V* approach. Anyway, the differences between the two approaches are small. The series resistance values obtained for the curves without additional resistance are in line with the results of Fig. 12 obtained for the same NP190GK module.

In order to further demonstrate the quality of the series resistance values identification, the average increases of the identified series resistances for the curves measured with additional resistances compared to the curves without any additional resistance are listed in Table 6 for all the four fitting approaches. The results of Table 6 show that the additional resistance values are identified accurately. Especially, the additional series resistances are very well identified by the *V* approach, for which the identified series resistances differ only 0.01 and 0.001 Ω from the used additional resistance values.

4. Discussion

In order to conclude the results, rankings of the studied approaches in several features are compiled in Table 7. The approaches were compared in terms of accurate identification of *G* and *T*, stable identification of the parasitic resistances, accuracy of curve fitting and computation costs based on the results of Section 3.1. Moreover, the approaches were compared in terms of accurate identification of additional R_s based on the results of Section 3.3. Summary of Table 7 shows that the *I* and *I&V* approaches are the most usable ones for parametric identification. They were the best two approaches in every feature except in the accurate identification of *G* and additional R_s. The *V&I* approach was the best one in terms of the accurate identification of *G* and the *V* approach identified the additional R_s most accurately. Otherwise the *V* and *V&I* approaches provided the most unstable identified values and were the least accurate approaches in general. Based on the summary of Table 7 it is evident that the most suitable approach for parameter identification is dependent on the identified parameter.

Table 6
Average increases of the identified series resistances (Ω) for the curves with additional resistances compared to the curves without any additional resistance.

Approach	0.22 Ω	0.69 Ω
I	0.266	0.718
V	0.230	0.689
I&V	0.261	0.706
V&I	0.238	0.696

Table 7
Rankings of the studied fitting approaches in several features.

Feature	*I*	*V*	*I&V*	*V&I*
Accurate identification of *G*, 1st example	4th	2nd	3rd	1st
Accurate identification of *G*, 2nd example	4th	2nd	3rd	1st
Accurate identification of *T*, 1st example	1st	4th	2nd	3rd
Accurate identification of *T*, 2nd example	1st	4th	2nd	3rd
Stable identification of R_s and R_{sh}, 1st example	1st	4th	2nd	3rd
Stable identification of R_s and R_{sh}, 2nd example	1st	4th	2nd	3rd
Accurate identification of additional R_s	4th	1st	3rd	2nd
Accuracy of curve fitting, 1st example	1st	4th	2nd	3rd
Accuracy of curve fitting, 2nd example	2nd	4th	1st	3rd
Computation costs, 1st example	1st	2nd	3rd	4th
Computation costs, 2nd example	2nd	3rd	1st	4th

The two identification examples in Section 3.1 demonstrated the accuracy of the proposed procedure utilizing the whole measured *I*–*V* curves. Moreover, feasibility of the proposed procedure for online condition monitoring was demonstrated in Section 3.2 using only a subset of the experimental samples falling close to the MPP. Measured *I*–*V* curves of three different PV module types, including both monocrystalline and polycrystalline silicon PV modules, were used in these examples. Moreover, the measurements were performed at two different locations. The use of quite different datasets demonstrates that the proposed SDM parameter identification procedure is neither affected by geographic factors nor by some specific feature of the PV module, but it can be applied in different locations for different PV modules of several types.

Naturally, the identified irradiance and temperature values are not fully comparable with the measured ones. Firstly, the experimental irradiance values are measured from a single point beside the PV module and the incident irradiance is not completely constant over the surface of the module, but irradiance differences might occur. Thus, it is expected that there are some differences between the identified and measured irradiance values. As for the temperature, even larger differences can be expected due to thermal inertia of the PV module. Instead of working with the actual cell temperature, the back-sheet temperature was measured for all the modules. Thus, the effect of thermal inertia is significant causing a time lag between the identified and measured temperatures. As can be seen in Fig. 11, the changes in the measured module back-sheet temperature follow the changes in the identified temperature trend with some delay. Moreover, also temperature differences exist within the PV module: for example, cells in the center might be warmer than cells closest to the edge.

One factor affecting performance of the fitting approaches based on RMSE minimization is point distribution of the *I*–*V* curves, i.e., how large share of the points is on which side of the MPP. In an ideal situation, the points would be evenly distributed, but in practice that is rare. Relative RMSE of a single point might be of totally different scale depending whether it is calculated with respect to the current or voltage. In practice, on constant current region (left side of the MPP), small difference in current will lead to large difference in voltage. Similarly, on the right side of the MPP, small difference in voltage will lead to large difference in current. Thus, the selected fitting approach defines which part of the curve has the highest weight when minimizing the RMSE. All the studied *I*–*V* curves had most of the points on the left side of the MPP, i.e., at voltages lower than the MPP voltage. For the I-53 and ISF-145 modules, the shares of points on the left side of the MPP were around 60% and 55%, respectively. For the NP190GK module, the share of points varied between 58% and 75% increasing with decreasing

irradiance (SC current) level.

In this study, the fitting approaches were compared using solely the proposed SDM parameter identification procedure. However, it was found in [28] that the most suitable fitting approach is dependent on the procedure used to compute the *I–V* curve from the SDM. Thus, further comparison of the fitting approaches based on RMSE minimization, especially the most promising ones (the *I* and *I&V* approaches), with several parameter identification procedures, considering both the SDM and two-diode model, is an interesting topic for future investigations.

5. Conclusions

This article proposed a novel procedure for SDM parameter identification from measured *I–V* curves without needing any other measurements. The only inputs of the proposed procedure are the *I–V* curve measurements from actual operating conditions among with the STC parameter values of the module. The proposed procedure identifies the SDM parameter values along with the operating irradiance and temperature values. Measured *I–V* curves of three PV module types from two different locations were used to experimentally validate the proposed procedure. First, accuracy of the proposed procedure when entire measured *I–V* curves are utilized was demonstrated by two identification examples. The examples show that the procedure identifies the operating irradiance and temperature of the PV modules with high accuracy even during sharp irradiance transitions and low irradiance conditions. Moreover, the identified series and shunt resistances were very stable under nearly constant high irradiance conditions. Especially, the proposed procedure was found to provide more stable identified values of the shunt resistance than an earlier method. Moreover, feasibility of the proposed procedure for online condition monitoring was demonstrated using only partial curves. The results show that the SDM parameters as well as the operating irradiance and temperature can be identified quite accurately from a small part of *I–V* curve measured in the vicinity of the MPP. This is an important finding demonstrating the feasibility of condition monitoring with only minimal interruption of PV power production. Moreover, *I–V* curve measurements with additional series resistance were used to demonstrate the correctness of the identified series resistance values.

Moreover, for the first time, a comprehensive comparison of various fitting approaches based on RMSE minimization was presented. In addition to the traditional *I* approach and earlier presented *V* approach, two novel approaches combining them were proposed. Our assumption was that applying different approaches for the left and right side of the MPP might be advantageous for identifying the parasitic resistances. The results show that the selected fitting approach affects the obtained parameter values. The *I* and *I&V* approaches were found to be the most usable ones giving the most stable identified values. Moreover, these approaches identified temperature most accurately and were the most accurate ones in terms of the area between the measured and fitted curves. However, these approaches showed the largest overestimation of the irradiance. On the other hand, the *V* approach provided the most accurate identified values of the additional series resistances although otherwise it provided the most unstable identified values and was shown to be the least accurate approach in general. The *V&I* approach was found to the best one in terms of the accurate identification of irradiance. However, it has the highest computational burden. Thus, the most suitable approach for parameter identification is dependent on the identified parameter. Based on the results it is evident that the used fitting approach is a factor that should be considered when implementing SDM parameter identification by curve fitting.

CRediT authorship contribution statement

Kari Lappalainen: Conceptualization, Data curation, Methodology, Formal analysis, Writing – original draft. **Michel Piliougine:** Conceptualization, Data curation, Writing – review & editing. **Giovanni Spagnuolo:** Conceptualization, Writing – review & editing.

Declaration of Competing Interest

The authors declare that they have no known competing financial interests or personal relationships that could have appeared to influence the work reported in this paper.

Acknowledgments

The work has received financial support from Business Finland and the "Ministerio de Ciencia, Innovación y Universidades" of the "Government of Spain" (grant RTI2018-095097-B-I00). The authors acknowledge Prof. Mariano Sidrach-de-Cardona from the University of Malaga for having made available some experimental data sets used in the article.

References

[1] Huerta Herraiz Á, Pliego Marugán A, García Márquez FP. Photovoltaic plant condition monitoring using thermal images analysis by convolutional neural network-based structure. Renewable Energy 2020;153:334–48. https://doi.org/10.1016/j.renene.2020.01.148.
[2] García Márquez FP, Ramírez IS. Condition monitoring system for solar power plants with radiometric and thermographic sensors embedded in unmanned aerial vehicles. Measurement 2019;139:152–62. https://doi.org/10.1016/j.measurement.2019.02.045.
[3] Yadir S, Bendaoud R, EL-Abidi A, Amiry H, Benhmida M, Bounouar S, et al. Evolution of the physical parameters of photovoltaic generators as a function of temperature and irradiance: New method of prediction based on the manufacturer's datasheet. Energy Convers Manage 2020;203:112141. https://doi.org/10.1016/j.enconman.2019.112141.
[4] Rusen SE, Konuralp A. Quality control of diffuse solar radiation component with satellite-based estimation methods. Renewable Energy 2020;145:1772–9. https://doi.org/10.1016/j.renene.2019.07.085.
[5] Blaga R, Calinoiu D, Stefu N, Boata R, Sabadus A, Paulescu E, et al. Quantification of the aerosol-induced errors in solar irradiance modeling. Meteorol Atmos Phys 2021;133(4):1395–407. https://doi.org/10.1007/s00703-021-00815-z.
[6] Hejri M, Mokhtari H. On the comprehensive parametrization of the photovoltaic (PV) cells and modules. IEEE J Photovoltaics 2017;7:250–8. https://doi.org/10.1109/JPHOTOV.2016.2617038.
[7] Batzelis EI, Papathanassiou SA. A method for the analytical extraction of the single-diode PV model parameters. IEEE Trans Sustainable Energy 2016;7:504–12. https://doi.org/10.1109/TSTE.2015.2503435.
[8] Abdel-Basset M, Mohamed R, Chakrabortty RK, Sallam K, Ryan MJ. An efficient teaching-learning-based optimization algorithm for parameters identification of photovoltaic models: Analysis and validations. Energy Convers Manage 2021;227:113614. https://doi.org/10.1016/j.enconman.2020.113614.
[9] Li S, Gu Q, Gong W, Ning B. An enhanced adaptive differential evolution algorithm for parameter extraction of photovoltaic models. Energy Convers Manage 2020;205:112443. https://doi.org/10.1016/j.enconman.2019.112443.
[10] Yu S, Heidari AA, Liang G, Chen C, Chen H, Shao Q. Solar photovoltaic model parameter estimation based on orthogonally-adapted gradient-based optimization. Optik 2022;252:168513. https://doi.org/10.1016/j.ijleo.2021.168513.
[11] Abbassi A, Ben Mehrez R, Touaiti B, Abualigah L, Touti E. Parameterization of photovoltaic solar cell double-diode model based on improved arithmetic optimization algorithm. Optik 2022;253:168600. https://doi.org/10.1016/j.ijleo.2022.168600.
[12] Panchal AK. *I-V* Data Operated High-Quality Photovoltaic Solution Through Per-Unit Single-Diode Model. IEEE J Photovoltaics 2020;10:1175–84. https://doi.org/10.1109/JPHOTOV.2020.2996711.
[13] Lappalainen K, Manganiello P, Piliougine M, Spagnuolo G, Valkealahti S. Virtual Sensing of Photovoltaic Module Operating Parameters. IEEE J Photovoltaics 2020;10:852–62. https://doi.org/10.1109/JPHOTOV.2020.2972688.
[14] Singh R, Sharma M, Rawat R, Banerjee C. An assessment of series resistance estimation techniques for different silicon based SPV modules. Renew Sustain Energy Rev 2018;98:199–216. https://doi.org/10.1016/j.rser.2018.09.020.
[15] Spataru S, Sera D, Kerekes T, Teodorescu R. Diagnostic method for photovoltaic systems based on light *I-V* measurements. Sol Energy 2015;119:29–44. https://doi.org/10.1016/j.solener.2015.06.020.
[16] Jain A, Kapoor A. Exact analytical solutions of the parameters of real solar cells using Lambert *W*-function. Sol Energy Mater Sol Cells 2004;81:269–77. https://doi.org/10.1016/j.solmat.2003.11.018.
[17] Hao P, Zhang Y, Lu H, Lang Z. A novel method for parameter identification and performance estimation of PV module under varying operating conditions. Energy Convers Manage 2021;247:114689. https://doi.org/10.1016/j.enconman.2021.114689.
[18] Oliva D, Cuevas E, Pajares G. Parameter identification of solar cells using artificial bee colony optimization. Energy 2014;72:93–102. https://doi.org/10.1016/j.energy.2014.05.011.

[19] Chin VJ, Salam Z. A New Three-point-based Approach for the Parameter Extraction of Photovoltaic Cells. Appl Energy 2019;237:519–33. https://doi.org/10.1016/j.apenergy.2019.01.009.
[20] Chin VJ, Salam Z, Ishaque K. Cell modelling and model parameters estimation techniques for photovoltaic simulator application: A review. Appl Energy 2015;154:500–19. https://doi.org/10.1016/j.apenergy.2015.05.035.
[21] Yu K, Liang JJ, Qu BY, Cheng Z, Wang H. Multiple learning backtracking search algorithm for estimating parameters of photovoltaic models. Appl Energy 2018;226:408–22. https://doi.org/10.1016/j.apenergy.2018.06.010.
[22] Patel SJ, Panchal AK, Kheraj V. Extraction of solar cell parameters from a single current–voltage characteristic using teaching learning based optimization algorithm. Appl Energy 2014;119:384–93. https://doi.org/10.1016/j.apenergy.2014.01.027.
[23] Tong NT, Pora W. A parameter extraction technique exploiting intrinsic properties of solar cells. Appl Energy 2016;176:104–15. https://doi.org/10.1016/j.apenergy.2016.05.064.
[24] Villalva MG, Gazoli JR, Filho ER. Comprehensive Approach to Modeling and Simulation of Photovoltaic Arrays. IEEE Trans Power Electron 2009;24:1198–208. https://doi.org/10.1109/TPEL.2009.2013862.
[25] Petrone G, Ramos-Paja CA, Spagnuolo G. Photovoltaic Sources Modeling. Chichester, United Kingdom: John Wiley & Sons; 2017.
[26] Batzelis E. Non-Iterative Methods for the Extraction of the Single-Diode Model Parameters of Photovoltaic Modules: A Review and Comparative Assessment. Energies 2019;12:358. https://doi.org/10.3390/en12030358.
[27] Piliougine M, Guejia-Burbano RA, Petrone G, Sanchez-Pacheco FJ, Mora-Lopez L, Sidrach-de-Cardona M. Parameters extraction of single diode model for degraded photovoltaic modules. Renewable Energy 2021;164:674–86. https://doi.org/10.1016/j.renene.2020.09.035.
[28] Mathew LE, Panchal AK. A Complete Numerical Investigation on Implicit and Explicit PV Single-Diode-Models Using I- and V-Approaches. IEEE J Photovoltaics 2021;11:827–37. https://doi.org/10.1109/JPHOTOV.2021.3067442.
[29] Eicker U. In: Solar Technologies for Buildings. Chichester, United Kingdom: John Wiley & Sons; 2003.
[30] De Soto W, Klein SA, Beckman WA. Improvement and validation of a model for photovoltaic array performance. Sol Energy 2006;80:78–88. https://doi.org/10.1016/j.solener.2005.06.010.
[31] Femia N, Petrone G, Spagnuolo G, Vitelli M. Power Electronics and Control Techniques for Maximum Energy Harvesting in Photovoltaic Systems. Boca Raton, USA: Taylor & Francis Group; 2013.
[32] Wilcox JR, Haas AW, Gray JL, Schwartz RJ. Estimating Saturation Current Based on Junction Temperature and Bandgap. AIP Conf Proc 2011;1407:30–3. https://doi.org/10.1063/1.3658288.
[33] Piliougine M, Carretero J, Mora-Lopez L, Sidrach-de-Cardona M. Experimental system for current–voltage curve measurement of photovoltaic modules under outdoor conditions. Prog Photovolt Res Appl 2011;19:591–602. https://doi.org/10.1002/pip.1073.
[34] Duran E, Piliougine M, Sidrach-de-Cardona M, Galan J, Andujar JM. Different methods to obtain the *I–V* curve of PV modules: A review. In Proceedings of 2008 33rd IEEE Photovoltaic Specialists Conference. https://doi.org/10.1109/PVSC.2008.4922578.
[35] Kalliojärvi-Viljakainen H, Lappalainen K, Valkealahti S. Preprocessing of PV Panel Measured Current-Voltage Characteristics Before Curve Fitting. In Proceedings of 2020 47th IEEE Photovoltaic Specialists Conference, p. 117–123. https://doi.org/10.1109/PVSC45281.2020.9300445.
[36] Torres Lobera D, Mäki A, Huusari J, Lappalainen K, Suntio T, Valkealahti S. Operation of TUT Solar PV Power Station Research Plant under Partial Shading Caused by Snow and Buildings. Int J Photoenergy 2013;2013:1–13. https://doi.org/10.1155/2013/837310. 837310.
[37] Piliougine M, Oukaja A, Sidrach-de-Cardona M, Spagnuolo G. Temperature coefficients of degraded crystalline silicon photovoltaic modules at outdoor conditions. Prog Photovolt Res Appl 2021;29:558–70. https://doi.org/10.1002/pip.3396.
[38] Kalliojärvi-Viljakainen H, Lappalainen K, Valkealahti S. A novel procedure for identifying the parameters of the single-diode model and the operating conditions of a photovoltaic module from measured current–voltage curves. Energy Reports 2022 (accepted for publication). https://authors.elsevier.com/tracking/article/details.do?aid=3573&jid=EGYR&surname=Kallioj%C3%A4rvi-Viljakainen.
[39] Hansen CW. Parameter Estimation for Single Diode Models of Photovoltaic Modules. SAND2015-2065. Albuquerque and Livermore, USA: Sandia National Laboratories; 2015.
[40] Spagnuolo G, Lappalainen K, Valkealahti S, Manganiello P. Identification and Diagnosis of a Photovoltaic Module Based on Outdoor Measurements. In Proceedings of 2019 IEEE Milan PowerTech. https://doi.org/10.1109/PTC.2019.8810767.